Advanced Studies in Contemporary Mathematics
36 (2026), No. 4, pp. 319 – 332

www.jangjeon.or.kr
http://dx.doi.org/10.17777/ascm2026.36.4.005

NUMERICAL ANALYSIS OF NONLINEAR CONVECTIVE MHD CASSON FLUID FLOW SUBJECT TO RADIATION AND EXPONENTIAL HEAT SOURCE OVER CONE

K.M MANJULA AND P.B. SAMPATH KUMAR

Abstract. The present study investigates the magnetohydrodynamic (MHD) mixed convection flow and heat transfer characteristics of a Casson fluid over a cone in the presence of thermal radiation, nonlinear thermal buoyancy, and exponential internal heat generation. The governing boundary-layer equations are transformed into a system of nonlinear ordinary differential equations using suitable similarity transformations. The resulting boundary value problem is solved numerically by employing the shooting technique together with the adaptive fourth-fifth order Runge-Kutta (RK45) method. The effects of the magnetic parameter, mixed convection parameter, Casson parameter, thermal radiation parameter, heat source parameter, exponential heat generation parameter, and nonlinear buoyancy parameter on the velocity and temperature distributions are examined. The numerical results reveal that increasing the magnetic parameter suppresses the fluid velocity owing to the enhanced Lorentz force, whereas the mixed convection parameter accelerates the flow. The temperature distribution increases with increasing thermal radiation, heat source, and exponential heat generation parameters due to enhanced thermal energy within the boundary layer. Furthermore, the influences of the governing parameters on the skin-friction coefficient and the local Nusselt number are presented and discussed. The present results provide useful insight into heat transfer enhancement in non-Newtonian Casson fluids over cone geometries encountered in polymer processing, thermal manufacturing, cooling systems, and other engineering applications.

2010 Mathematics Subject Classification. 00A00, 00B00, 00C00.

Keywords and phrases. solar radiation; Casson fluid; exponential internal heat source; magnetic field.

1. INTRODUCTION

In recent years, non-Newtonian fluid mechanics has attracted considerable attention due to its extensive applications in science and engineering. Unlike Newtonian fluids, whose viscosity remains constant, non-Newtonian fluids exhibit complex rheological characteristics that depend on the applied shear rate or stress. Common examples include blood, polymer melts, lubricating oils, honey, toothpaste, shampoos, paints, ketchup, sugar solutions, drilling muds, and various industrial suspensions. Owing to the diverse rheological responses exhibited by these materials, no single constitutive equation can adequately describe all categories of non-Newtonian fluids. Consequently,

The authors declare that they have no conflict of interest. There are no funders to report for this submission.

numerous mathematical models have been proposed, each designed to represent a specific class of fluid behavior. Among these models, the Casson fluid model has gained significant importance because of its capability to characterize yield stress effects. According to this model, the material behaves as a rigid body when the applied shear stress is lower than the yield stress, whereas it begins to flow once the applied stress exceeds the yield limit. This characteristic makes the Casson model suitable for describing the behavior of several biological and industrial fluids. Several researchers have investigated the transport characteristics of Casson fluids under different physical conditions. Ullah et al. [1] analyzed magnetohydrodynamic slip flow of a Casson fluid over a nonlinear stretching surface embedded in a porous medium with Newtonian heating. Girish et al. [2] examined the MHD nonlinear convective flow of Carreau-Casson fluids over a deformable surface in the presence of homogeneous and heterogeneous chemical reactions. Their model incorporated nonlinear thermal radiation together with Joule heating. Rauf et al. [3] examined the thermal and concentration transport of Casson nanofluid over a bidirectional stretching sheet subjected to convective boundary conditions. Abbas et al. [4] presented a numerical study of stagnation-point flow of a chemically reactive Casson fluid. Raju et al. [5] explored heat and mass transfer in an exponentially stretching Casson fluid flow. Ahmadpour et al. [6] studied the unsteady squeezing flow and radiative heat transfer of Casson fluids in the presence of non-uniform heat generation/absorption and suction/injection, and obtained analytical solutions using the Homotopy Perturbation Method. Sampath et al. [7] examined the three-dimensional MHD flow and heat transfer of a Casson-Williamson nanofluid over a stretching surface. Their results revealed that increasing the magnetic parameter significantly reduced the fluid velocity while enhancing the temperature distribution. Very recently, the flow characteristics of Casson fluid have attracted considerable attention from researchers [8-11]. These studies have explored the effects of different physical parameters on momentum and heat transfer, contributing significantly to the understanding of Casson fluid dynamics in engineering and industrial applications.

Flow over conical geometries has attracted significant attention owing to its wide range of engineering and industrial applications, such as aerospace engineering, thermal insulation systems, nuclear reactors, heat exchangers, cooling of electronic devices, and chemical processing. The unique geometry of a cone influences the boundary-layer development and transport characteristics, making it an important configuration for studying fluid flow and heat transfer. Consequently, numerous theoretical and numerical investigations have been conducted to understand the behavior of fluids over cones under different thermal and physical conditions. Very recently, several researchers [12-18] have examined cone flow by incorporating the effects of magnetic fields, thermal radiation, porous media, viscous dissipation, slip conditions, and convective heating. Their findings revealed that these physical parameters significantly alter the velocity, temperature, and concentration profiles, thereby providing valuable insights into optimizing heat and mass transfer in practical engineering systems.

Mixed convection refers to a heat transfer mechanism in which fluid motion is generated by the combined action of externally imposed forces and buoyancy forces resulting from temperature-induced density variations. In this mode of transport, both forced and free convection contribute simultaneously to the overall flow behavior. Such phenomena are frequently encountered in numerous engineering and industrial applications, including solar thermal collectors, electronic cooling systems, thermal energy storage units, cryogenic processes, and nuclear reactor cooling. Because of its broad practical relevance, mixed convection has attracted sustained research interest, leading to extensive investigations under different flow configurations and thermal conditions [19-26]. In many practical situations involving large temperature gradients, the commonly adopted linear approximation for the relationship between fluid density and temperature becomes inadequate. Under these circumstances, higher-order temperature-dependent density variations must be considered, giving rise to nonlinear mixed convection. The inclusion of nonlinear buoyancy effects significantly modifies the flow structure as well as the associated heat transfer characteristics. These effects are particularly important in several technological and industrial processes, such as geothermal energy extraction, heat pump systems, combustion technology, natural gas production, refrigeration equipment, and pharmaceutical manufacturing. Recognizing the importance of nonlinear buoyancy, Kameswaran et al. [27] examined boundary-layer flow through a porous medium over a vertical surface by incorporating nonlinear convection together with thermophoretic transport. Hayat et al. [28] investigated the three-dimensional mixed convection flow of a Sisko nanofluid over an elastic stretching surface while accounting for both thermal and solutal buoyancy effects. Khan et al. [29] analyzed entropy generation in the nonlinear mixed convection flow of a tangent hyperbolic nanofluid over an expanding surface and demonstrated that increasing the nonlinear convection parameter enhances the fluid velocity. Irfan [30] further explored magnetohydrodynamic nonlinear mixed convection in a Carreau nanofluid with variable thermophysical properties. In addition, the influence of nonlinear convection on fluid flow and thermal transport under diverse physical conditions has been reported in several subsequent studies by Idowu et al. [31], Ibrahim and Kenea [32], Kenea and Ibrahim [33], and Reddy et al. [34].

Although numerous studies have been carried out on MHD non-Newtonian fluid flows, most existing investigations are limited to stretching surfaces and conventional thermal models involving linear buoyancy and uniform heat generation. The combined effects of nonlinear thermal buoyancy, thermal radiation, and exponential internal heat generation on Casson fluid flow over cone geometries have received relatively limited attention. Since these mechanisms play a crucial role in controlling momentum and heat transport in practical thermal systems, a comprehensive analysis is required. Therefore, the present study aims to bridge this gap by exploring the MHD mixed convection behavior of Casson fluid over a cone, considering the coupled effects of radiation and nonlinear heat generation to provide deeper insights into flow dynamics and thermal performance.

2. PROBLEM STATEMENT

Consider the steady, two-dimensional magnetohydrodynamic (MHD) mixed convection boundary-layer flow of an incompressible Casson fluid over a cone. A uniform magnetic field of strength (B_0) is applied normal to the cone surface. The effects of thermal radiation, nonlinear thermal buoyancy, uniform heat source, and exponential internal heat generation are taken into account. The induced magnetic field is assumed to be negligible due to a small magnetic Reynolds number, and viscous dissipation and Joule heating are neglected. The fluid is assumed to be electrically conducting, and all thermophysical properties are considered constant except for the density variation appearing in the buoyancy term under the Boussinesq approximation. It is assumed that γ is the cone or wedge half angle and r is the radius of the cone. Under the above assumptions, the governing partial differential equations are:

Continuity.

$$\frac{\partial(r^m u)}{\partial x} + \frac{\partial(r^m v)}{\partial y} = 0. \tag{2.1}$$

Momentum.

$$u\frac{\partial u}{\partial x}+v\frac{\partial u}{\partial y} = \nu\left(1+\frac{1}{\beta}\right)\frac{\partial^2 u}{\partial y^2}+g\left[\beta_1(T-T_\infty)+\beta_2(T-T_\infty)^2\right]\cos\gamma-\frac{\sigma B_0^2}{\rho}u. \tag{2.2}$$

Energy.

$$u\frac{\partial T}{\partial x}+v\frac{\partial T}{\partial y} = \alpha_m\frac{\partial^2 T}{\partial y^2}-\frac{1}{\rho c_p}\frac{\partial q_r}{\partial y}+\frac{Q_t}{\rho c_p}(T-T_\infty)+\frac{Q_e}{\rho c_p}(T_w-T_\infty)\exp\left(\frac{-n}{l}y\right), \tag{2.3}$$

The boundary conditions are defined by:

$$u = u_w = \frac{\upsilon x}{l^2}, \quad v = 0, \quad T = T_w, \quad C = C_w \quad \text{at } y = 0, \tag{1}$$

$$u \to 0, \quad T \to T_\infty, \quad C \to C_\infty \quad \text{as } y \to 0, \tag{2.4}$$

here u and v are velocity components along x and y directions respectively, β is the Casson fluid parameter, T and C are temperature and nanoparticles volume fraction respectively, υ is the kinematic viscosity, μ is the dynamic viscosity, σ is the electrical conductivity, ρ density of fluid, B_0 is the magnetic field strength, β_1, β_2 are thermal diffusivities, g is the acceleration due to gravity, $\alpha_m = k/\rho c_p$ is the thermal diffusivity of the fluid, k is the thermal conductivity, c_p is specific heat, $\tau = (\rho c)_p/(\rho c)_f$ is the ratio of the effective heat capacity of nanoparticles and the heat capacity of ordinary fluid, Q_t is the thermal dependent heat source coefficient, Q_e is the exponential space dependent heat source coefficient and q_r is the radiative heat flux.

The energy equation takes the following form in view of Rosseland approximation:

$$u\frac{\partial T}{\partial x}+v\frac{\partial T}{\partial y} = \alpha_m\frac{\partial^2 T}{\partial y^2}+\frac{\partial}{\partial y}\left(\frac{16\sigma^*}{3k^*\rho c_p}T^3\frac{\partial T}{\partial y}\right)+\frac{Q_t}{\rho c_p}(T-T_\infty)+\frac{Q_e}{\rho c_p}(T_w-T_\infty)e^{\frac{-n}{l}y}, \tag{2.5}$$

where σ^* and k^* are the Stefan-Boltzmann constant and mean absorption coefficient respectively.

Now introduce the stretching transformations:

(2.6)
$$\eta = \frac{u_w l}{xv} y, \quad u = \frac{vx}{l} f'(\eta), \quad v = \frac{v(m+1)}{l} f(\eta), \quad T = T_\infty + \theta(\eta)(T_w - T_\infty),$$

here l is characteristic length and prime denotes differentiation with respect to η.

Using (2.6) in (2.1)-(2.5) we have:

$$\left(1 + \frac{1}{\beta}\right) f''' + (m+1) f f'' - f'^2 + Gr\left(\theta + \alpha_1 \theta^2\right) \cos\gamma - M f' = 0, \tag{2.7}$$

$$\frac{1 + Rd}{\Pr} \theta'' + (m+1) f \theta' + Q_t \theta + Q_E e^{-n\eta} = 0. \tag{2.8}$$

with the boundary conditions:

$$f(0) = 0, \quad f'(0) = 1, \quad \theta(0) = 1, \tag{2}$$

$$f'(\infty) = 0, \quad \theta(\infty) = 0, \tag{2.9}$$

In the above equations Gr, α_1, M, Pr, Rd, Q_t, Q_E, are correspondingly Grashof number, thermal nonlinear convection parameter, magnetic parameter, Prandtl number, radiation parameter, thermal dependent heat source/sink parameter and exponential space dependent heat source/sink parameter. They are given below:

$$Gr = \frac{gl^2 \beta_1 (T_w - T_\infty)}{v u_w}, \quad \alpha_1 = \frac{\beta_2 (T_w - T_\infty)}{\beta_1}, \tag{3}$$

$$M = \frac{\sigma B_0^2 l^2}{\rho v}, \quad \Pr = \frac{v}{\alpha_m}, \tag{4}$$

$$Rd = \frac{16\sigma^* T^3}{3k^* k}, \quad Q_T = \frac{Q_t l^2}{\mu c_p}, \quad Q_E = \frac{Q_e l^2}{\mu c_p} \tag{5}$$

It is worth mentioning that the present investigation is confined to the **cone geometry**. Accordingly, the analysis is performed by taking the wedge parameter $m = 1$ with a non-zero cone half-angle ($\gamma \neq 0$), which represents the steady boundary-layer flow over a cone.

The friction factor, Nusselt number and Sherwood number are:

$$C_f = \left(1 + \frac{1}{\beta}\right) f''(0), \tag{2.10}$$

$$Nu = -(1 + Rd)\theta'(0), \tag{2.11}$$

3. NUMERICAL PROCEDURE

The nonlinear coupled ordinary differential equations (2.7) and (2.8), together with the corresponding boundary conditions, are solved numerically using the shooting method combined with the adaptive fourth-fifth order Runge-Kutta (RK45) integration scheme implemented in the Python SciPy

library. To facilitate the numerical computation, the higher-order differential equations are first transformed into a system of first-order ordinary differential equations by introducing the following dependent variables:

$$y_1 = f, \quad y_2 = f', \quad y_3 = f'', \quad y_4 = \theta, \quad y_5 = \theta'.$$

Accordingly, the governing equations are rewritten as:

$$\frac{dy_1}{d\eta} = y_2, \tag{6}$$

$$\frac{dy_2}{d\eta} = y_3, \tag{7}$$

$$\frac{dy_3}{d\eta} = \frac{-(m+1)y_1y_3 + y_2^2 - Gr\left(y_4 + \alpha_1 y_4^2\right)\cos\gamma + My_2}{1+\frac{1}{\beta}}, \tag{8}$$

$$\frac{dy_4}{d\eta} = y_5, \tag{9}$$

$$\frac{dy_5}{d\eta} = -\frac{\Pr}{1+Rd}\left[(m+1)y_1y_5 + Q_t y_4 + Q_E e^{-n\eta}\right]. \tag{10}$$

with the boundary conditions:

$$f(0) = 0, \quad f'(0) = 1, \quad \theta(0) = 1, \tag{11}$$

$$f'(\infty) = 0, \quad \theta(\infty) = 0, \tag{12}$$

The corresponding initial conditions are:

$$y_1(0) = 0, \quad y_2(0) = 1, \quad y_4(0) = 1, \tag{13}$$

while the unknown initial slopes:

$$y_3(0) = f''(0), \quad y_5(0) = \theta'(0) \tag{14}$$

are determined iteratively using the shooting technique.

The computational domain is truncated to a finite boundary, $\eta_\infty = 8$, which is sufficiently large to satisfy the asymptotic boundary conditions. Initial guesses are assigned for the unknown quantities $f''(0)$ and $\theta'(0)$. For each set of guessed values, the resulting initial value problem is integrated from $\eta = 0$ to $\eta = 8$ using the adaptive RK45 algorithm. The numerical solution at the far-field boundary is then compared with the required boundary conditions. The nonlinear root-finding algorithm updates the guessed values until the convergence criteria:

$$|f'(\eta_\infty)| < 10^{-6}, \quad |\theta(\eta_\infty)| < 10^{-6} \tag{15}$$

are simultaneously satisfied. After achieving convergence, the velocity and temperature profiles are obtained for various values of the governing parameters.

To validate the accuracy of the present numerical method, the computed values of the skin-friction coefficient, $(-f''(0))$, are compared with the previously published results of Cortell [35] and Tufail et al. [36] for the special case $(\beta \to \infty)$, $(Gr = 0)$, and $(m = 0)$. The comparison, presented in Table 1, demonstrates excellent agreement between the present results and the existing literature, thereby confirming the accuracy, stability, and reliability of the numerical procedure employed in this study.

TABLE 1. Comparison of the present values of the skin-friction coefficient, $(-f''(0))$, with the results of Cortell [35] and Tufail et al. [36] for the special case $(\beta \to \infty)$, $(Gr = 0)$, and $(m = 0)$.

M	$-\mathbf{f''(0)}$ **Cortell [35]**	$-\mathbf{f''(0)}$ **Tufail et al. [36]**	$-\mathbf{f''(0)}$ **Present study**	$\theta'(\mathbf{0})$ **Present study**
0	1.00000	1.00000	1.00001	2.32634
0.5	1.22475	1.22474	1.22468	5.76077
1	1.41421	1.41421	1.41414	-12.2825
1.5	1.58114	1.58114	1.58105	-1.45216
2	1.73205	1.73205	1.73196	-1.04649
2.5	-	1.87083	1.87073	-0.04929
3	-	2.00000	1.99990	0.59329

4. RESULTS AND DISCUSSION

A parametric analysis was given to explore the consequences of embedded parameters on velocity $f'(\eta)$ and temperature $\theta(\eta)$. The friction factor C_f and Nusselt number Nu are also calculated. Unless otherwise stated, the numerical computations are carried out by fixing the governing parameters at the values $\beta = 2.0$, $m = 1$, $Gr = 0.8$, $\alpha_1 = 0.7$, $Pr = 6.2$, $Rd = 0.8$, $Q_t = 0.5$, $Q_E = 0.5$, and $n = 1.0$. In each graphical illustration, only one parameter is varied while all remaining parameters are maintained at these baseline values to clearly demonstrate its individual influence on the velocity and temperature distributions, as well as on the skin-friction coefficient and local Nusselt number.

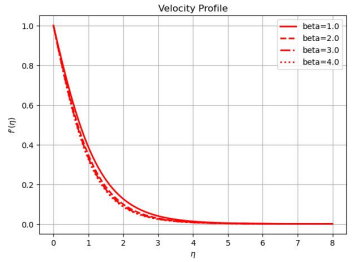


FIGURE 1. Effect of β on $f'(\eta)$

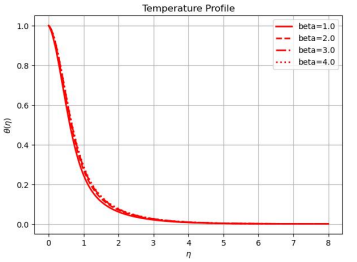


FIGURE 2. Effect of β on $\theta(\eta)$

Effect of Casson Parameter. Figure 1 depicts the influence of the Casson parameter, (β), on the dimensionless velocity profile $f'(\eta)$. It is observed that the velocity decreases with increasing values of the Casson parameter. The increase in (β) enhances the fluid's resistance to motion in the present model, thereby suppressing the fluid velocity and reducing the momentum boundary-layer thickness. Figure 2 illustrates the effect of the Casson parameter, (β), on the temperature profile $\theta(\eta)$. It is evident that the temperature increases as the Casson parameter increases. The reduction in fluid

velocity weakens convective heat transport from the cone surface, allowing more heat to remain within the thermal boundary layer. Consequently, the thermal boundary-layer thickness increases, leading to higher temperature distributions.

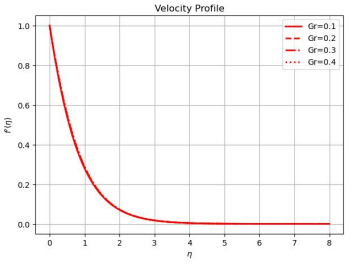


FIGURE 3. Effect of Gr on $f'(\eta)$

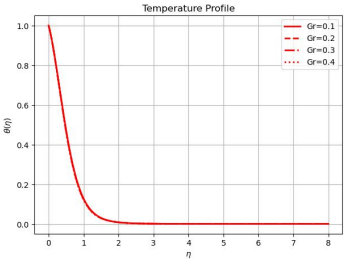


FIGURE 4. Effect of Gr on $\theta(\eta)$

Effect of Grashof Number. Figure 3 illustrates the influence of the Grashof number, (Gr), on the dimensionless velocity profile. It is observed that the velocity profile increases with increasing values of (Gr). Physically, a higher Grashof number signifies a stronger buoyancy force relative to the viscous force. The enhanced buoyancy accelerates the fluid flow along the cone surface, thereby increasing the velocity and thickening the momentum boundary layer. Figure 4 depicts the effect of the Grashof number on the temperature distribution. It is evident that the temperature decreases as (Gr) increases. The stronger buoyancy-induced flow enhances convective heat transport from the cone surface, resulting in a thinner thermal boundary layer and improved heat transfer characteristics.

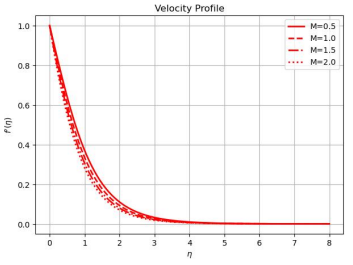


FIGURE 5. Effect of M on $f'(\eta)$

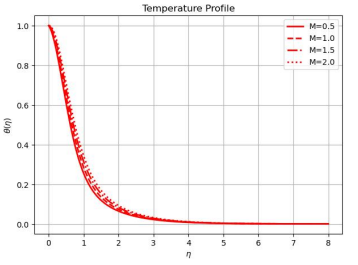


FIGURE 6. Effect of M on $\theta(\eta)$

Effect of Magnetic Parameter. Figures 5 and 6 illustrate the effects of the magnetic parameter (M) on the velocity and temperature profiles, respectively. It is observed that increasing (M) decreases the velocity while increasing the temperature. Physically, a stronger magnetic field generates a Lorentz force that opposes the fluid motion, thereby suppressing the velocity

and reducing the momentum boundary-layer thickness. The weakened fluid motion diminishes convective heat transfer from the cone surface, causing more thermal energy to be retained within the boundary layer. As a result, the temperature profile and thermal boundary-layer thickness increase with increasing values of the magnetic parameter.

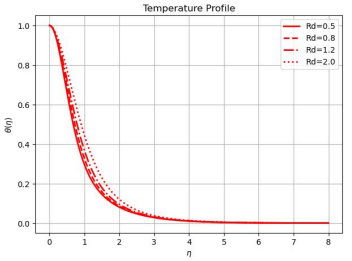


FIGURE 7. Effect of Rd on $\theta(\eta)$

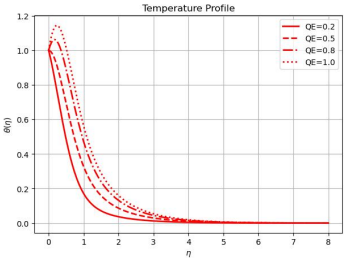


FIGURE 8. Effect of Q_E on $\theta(\eta)$

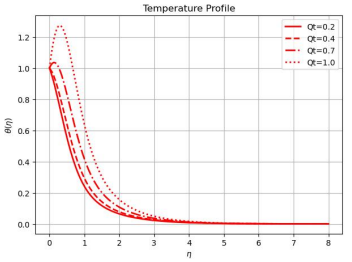


FIGURE 9. Effect of Q_t on $\theta(\eta)$

Effect of Radiation and Heat Source Parameters. Figure 7 illustrates the influence of the thermal radiation parameter (Rd) on the temperature profile. It is observed that the temperature increases with increasing values of (Rd), as thermal radiation supplies additional energy to the fluid, thereby thickening the thermal boundary layer. Figure 8 depicts the effect of the exponential heat generation parameter (Q_E) on the temperature distribution. An increase in (Q_E) enhances the internal heat generation within the fluid, resulting in higher temperature profiles and a thicker thermal boundary layer. Figure 9 shows the effect of the heat source parameter (Q_t) on the temperature profile. It is evident that increasing (Q_t) raises the fluid temperature by supplying additional thermal energy to the flow, which consequently increases the thermal boundary-layer thickness.

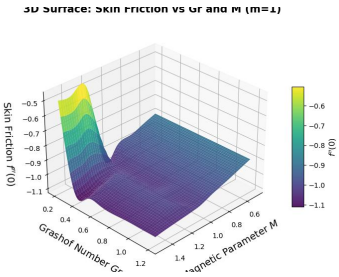


FIGURE 10. Effect of Gr and M on skin friction

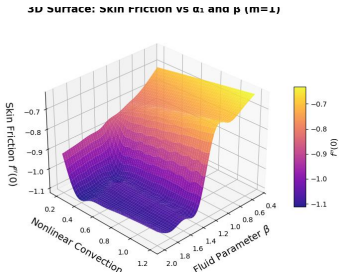


FIGURE 11. Effect of α_1 and β on skin friction

Skin Friction and Nusselt Number. Figures 10 and 11 present the combined effects of the governing parameters on the skin-friction coefficient $f''(0)$. Figure 10 shows the variation of skin friction with the magnetic parameter (M) and Grashof number (Gr). It is observed that increasing the magnetic parameter increases the magnitude of the skin-friction coefficient due to the resistive Lorentz force, whereas increasing the Grashof number reduces its magnitude as the buoyancy force assists the fluid motion and lowers the wall shear stress. Figure 11 illustrates the combined influence of the nonlinear convection parameter (α_1) and the Casson fluid parameter (β) on the skin-friction coefficient. The magnitude of the skin-friction coefficient increases with increasing (β), indicating greater wall shear stress, while an increase in (α_1) reduces the skin-friction coefficient owing to the enhancement of buoyancy-induced flow. These three-dimensional surfaces clearly demonstrate the coupled influence of the controlling parameters on the wall shear characteristics of the fluid flow.

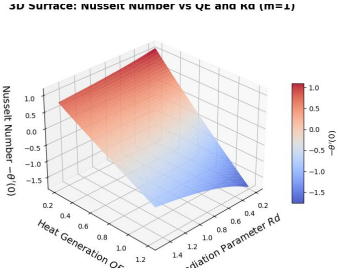


FIGURE 12. Effect of Q_E and Rd on Nusselt number

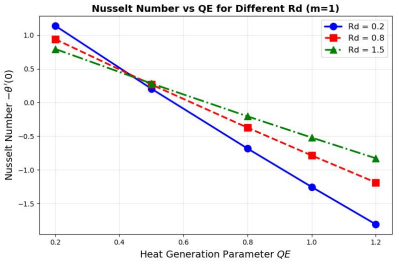


FIGURE 13. Effect of Rd on Nusselt number

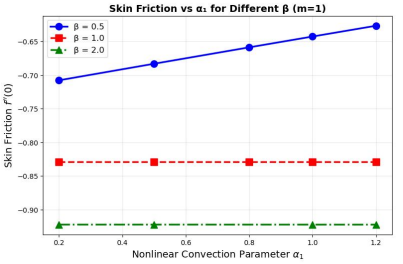


FIGURE 14. Effect of α and β on skin friction

Figure 12 illustrates the combined influence of the thermal radiation parameter (Rd) and exponential heat generation parameter (Q_E) on the local Nusselt number, $-\theta'(0)$. It is observed that increasing either (Rd) or (Q_E) decreases the Nusselt number. Physically, larger values of the radiation parameter enhance the thermal energy within the boundary layer, while higher exponential heat generation supplies additional internal heat to the fluid. Consequently, the wall temperature gradient decreases, leading to a reduction in the heat transfer rate at the cone surface. Therefore, the combined effects of thermal radiation and exponential heat generation significantly diminish the local Nusselt number.

5. CONCLUDING REMARKS

This study presents a numerical investigation of mixed convective magnetohydrodynamic Casson fluid flow over a cone in the presence of thermal radiation and exponential internal heat generation. The transformed nonlinear governing equations were solved using the shooting method coupled with the Runge-Kutta integration technique. The numerical results demonstrate that the fluid flow and thermal fields are strongly influenced by the governing physical parameters. An increase in the Casson parameter and magnetic parameter suppresses the fluid velocity, whereas the mixed convection parameter enhances the flow due to the buoyancy force. The thermal radiation parameter, exponential heat generation parameter, and heat source parameter elevate the fluid temperature and enlarge the thermal boundary layer. Consequently, the local Nusselt number decreases because the wall temperature gradient is weakened, while the skin friction coefficient exhibits a significant dependence on the flow parameters. The comparison with previously published results for a limiting case confirms the accuracy and reliability of the present numerical procedure. These findings provide useful insights into thermal management and transport processes involving non-Newtonian electrically conducting fluids in engineering systems such as thermal processing, polymer manufacturing, geothermal technologies, and energy conversion devices.

REFERENCES

[1] I. Ullah, S. Shafie, and I. Khan, Effects of slip condition and Newtonian heating on MHD flow of Casson fluid over a nonlinearly stretching sheet saturated in a porous medium, Journal of King Saud University-Science, 29, 250-259 (2017).

[2] Gireesha, B. J., P.B. Sampath Kumar, B. Mahanthesh, S. A. Shehzad, and A. Rauf. "Nonlinear 3D flow of Casson-Carreau fluids with homogeneous–heterogeneous reactions: a comparative study." *Results in physics* 7 (2017): 2762-2770.
[3] A. Rauf, M.K. Siddiq, F.M. Abbasi, M.A. Meraj, M. Ashraf, and S.A. Shehzad, Influence of convective conditions on three dimensional mixed convective hydromagnetic boundary layer flow of Casson nanofluid, Journal of Magnetism and Magnetic Materials, 416, 200-207 (2016).
[4] Z. Abbas, M. Sheikh, S.S. Motsa, Numerical solution of binary chemical reaction on stagnation point flow of Casson fluid over a stretching/shrinking sheet with thermal radiation, Energy, 95, 12-20 (2016).
[5] C.S.K. Raju, N. Sandeep, V. Sugunamma, M.J. Babu, and J.V.R. Reddy, Heat and mass transfer in magnetohydrodynamic Casson fluid over an exponentially permeable stretching surface, Engineering Science and Technology, an International Journal, 19, 45-52 (2016).
[6] A. Ahmadpour, M. Nasiri, M. Khazayinejad, and N. Asgharian, Flow and convective heat transfer of Casson fluid between squeezing porous disks in the presence of thermal radiation, viscous dissipation, and variable heat source/sink, Journal of the Brazilian Society of Mechanical Sciences and Engineering, 40(3), 135 (2018).
[7] Sampath Kumar, P. B. "Impact of Activation energy and chemical reaction on 3D MHD flow of Casson–Williamson Nanofluid." *International Journal of Mechanics and Materials in Design* 22, no. 2 (2026): 101.
[8] Sarki, Muhammad Nasiru, Abdullahi Sani Aleiro, Abubakar Sani Fakai, Muhammed Murtala Hamza, and Abdulsalam Shuaibu. "Fractional model for Casson fluid flow with thermal radiation effects in a convectively heated channel." *Multiscale and Multidisciplinary Modeling, Experiments and Design* 9, no. 1 (2026): 136.
[9] Abbas, Z., M. Kiran, M. Mujahid, and M. Y. Rafiq. "Rheological behavior of Casson fluid in pressure-driven flow through a wavy curved channel under Rosseland's approximation." *Physics of Fluids* 38, no. 1 (2026).
[10] Akram, Muhammad Javed, Haibiao Zheng, and Samad Noeiaghdam. "FEM Study of Nonlinear MHD Casson Nanofluid Flow with Thermo-Solutal Transport and Chemical Reaction Effects over a Vertical Stretching Surface." *International Journal of Thermofluids* (2026): 101639.
[11] D.L., Kiran Kumar, Divya, Bhargavi, and Malashri S. "Numerical modeling of magneto-thermo-solutal casson fluid flow over an exponentially stretching sheet using taylor wavelets." *Research in Mathematics* 13, no. 1 (2026): 2673645.
[12] Turkyilmazoglu, Mustafa. "On the fluid flow and heat transfer between a cone and a disk both stationary or rotating." *Mathematics and Computers in Simulation* 177 (2020): 329-340.
[13] Srilatha, Pudhari, Srinivas Remidi, Mulupuri Nagapavani, Harjot Singh, and B. C. Prasannakumara. "Heat and mass transfer analysis of a fluid flow across the conical gap of a cone-disk apparatus under the thermophoretic particles motion." *Energies* 16, no. 2 (2023): 952.
[14] Patil, P. M., and H. F. Shankar. "Double-diffusive nonlinear convection dusty fluid flow over a cone under the influence of activation energy: Double-diffusive nonlinear convection dusty fluid flow over a cone under the influence." *Indian Journal of Physics* 97, no. 9 (2023): 2771-2785.
[15] John, A. S., B. Mahanthesh, and G. Lorenzini. "Study of hybrid nanofluid flow in a stationary cone-disk system with temperature-dependent fluid properties." *Applied Mathematics and Mechanics* 45, no. 4 (2024): 677-694.
[16] Alshehry, Azzh Saad, Saima Noor, Syed Arshad Abas, Mehreen Fiza, and Hakeem Ullah. "Analysis of MHD hybrid nanofluid flow over cone and wedge with exponential and thermal heat source and activation energy." *Open Physics* 23, no. 1 (2025): 20250194.
[17] Bafe, Endale Ersino, Mitiku Daba Firdi, and Lemi Guta Enyadene. "Unsteady Williamson nanofluid flow over a rotating cone: effects of variable properties, thermal radiation, and chemical reactions." *International Journal of Thermofluids* 27 (2025): 101211.

[18] Patgiri, Indushri, and Utpal Jyoti Das. "Nanofluid flow across a vertical cone: effects of Hall current, Arrhenius energy, and heat radiation." *International Journal of Ambient Energy* 47, no. 1 (2026): 2620737.
[19] Reddy Gorla, R. S., & Sidawi, I. (1994). Free convection on a vertical stretching surface with suction and blowing. *Applied scientific research*, 52(3), 247-257.
[20] Chamkha, A. J. (1997). Non-Darcy fully developed mixed convection in a porous medium channel with heat generation/absorption and hydromagnetic effects. *Numerical Heat Transfer, Part A Applications*, 32(6), 653-675.
[21] Hayat, T., Abbas, Z., Pop, I., & Asghar, S. (2010). Effects of radiation and magnetic field on the mixed convection stagnation-point flow over a vertical stretching sheet in a porous medium. *International Journal of Heat and Mass Transfer*, 53(1-3), 466-474.
[22] Das, K. (2013). Mixed convection stagnation point flow and heat transfer of Cu-water nanofluids towards a shrinking sheet. *Heat Transfer—Asian Research*, 42(3), 230-242.
[23] Islam, S., Khan, A., Kumam, P., Alrabaiah, H., Shah, Z., Khan, W., ... & Jawad, M. (2020). Radiative mixed convection flow of Maxwell nanofluid over a stretching cylinder with joule heating and heat source/sink effects. *Scientific reports*, 10(1), 17823.
[24] Tulu, A., Hirpho, M., & Sohail, M. (2024). Modeling and simulation of mixed convection flow with viscous dissipation in a lid-driven hexagonal cavity using finite element method. *International Journal of Thermofluids*, 22, 100702.
[25] Al-Kaby, R. N., Abdulhaleem, S. M., Hameed, R. H., & Yasiry, A. (2025). Mixed convection heat transfer and fluid flow of nanofluid/porous medium under magnetic field influence. *Applied Sciences*, 15(3), 1087.
[26] Znaidia, S., Rehman, S., Drissi, N., Asiri, F., & Nasr, S. (2025). Mixed Convection Flow and Heat Transfer of Williamson Drilling Nanofluid Over a Stretching Cylinder Using Brinkman-Maxwell-Garnett Model and temperature-dependent Features. *Journal of Nonlinear Mathematical Physics*, 32(1), 78.
[27] Kameswaran, P. K., Sibanda, P., Partha, M. K., & Murthy, P. V. S. N. (2014). Thermophoretic and nonlinear convection in non-Darcy porous medium. *Journal of Heat Transfer*, 136(4), 042601.
[28] Hayat, T., Ullah, I., Alsaedi, A., Waqas, M., & Ahmad, B. (2017). Three-dimensional mixed convection flow of Sisko nanoliquid. *International Journal of Mechanical Sciences*, 133, 273-282.
[29] Khan, M. I., Khan, T. A., Qayyum, S., Hayat, T., Khan, M. I., & Alsaedi, A. J. T. E. P. J. P. (2018). Entropy generation optimization and activation energy in nonlinear mixed convection flow of a tangent hyperbolic nanofluid. *The European Physical Journal Plus*, 133(8), 329.
[30] Irfan, M. (2021). Study of Brownian motion and thermophoretic diffusion on nonlinear mixed convection flow of Carreau nanofluid subject to variable properties. *Surfaces and Interfaces*, 23, 100926.
[31] Idowu, A. S., Akolade, M. T., Oyekunle, T. L., & Abubakar, J. U. (2021). Nonlinear convection flow of dissipative Casson nanofluid through an inclined annular microchannel with a porous medium. *Heat transfer*, 50(4), 3388-3406.
[32] Ibrahim, W., & Kenea, G. (2024). Nonlinear convection flow of a micropolar nanofluid past a stretching sphere with convective heat transfer. *Journal of Nanofluids*, 13(2), 407-422.
[33] Kenea, G., & Ibrahim, W. (2024). Nonlinear convection stagnation point flow of Oldroyd-B nanofluid with non-Fourier heat and non-Fick's mass flux over a spinning sphere. *Scientific Reports*, 14(1), 841.
[34] Reddy, G. S. K., Raju, S. S. K., Mulki, H., & Souayeh, B. (2026). Nonlinear Convection of a Power-Law Fluid-Saturated Reactive Porous Layer. *Axioms*, 15(7), 487.
[35] R. Cortell, A note on magnetohydrodynamic flow of a power-law fluid over a stretching sheet, Appl. Math. Comput., 168, 557-566 (2005).
[36] M. N. Tufail, A. S. Butt and A. Ali, Heat source/sink effects on non-Newtonian MHD fluid flow and heat transfer over a permeable stretching surface: Lie group analysis, Indian. J. Phys., 88, 75-82 (2013).

Department of Mathematics, Government First Grade College, Channarayapatna-573225, Karnataka, India
Email address: manjulakm6640@gmail.com

Department of Studies and Research in Mathematics, Ramanagara PG Centre, Bangalore University, Karnataka 562159, India, Universidad Bernardo O'Higgins, Facultad de Ingeniería, Ciencia y Tecnología, Departamento de Formación y Desarrollo Científico en Ingeniería, Av. Viel 1497, Santiago, Chile
Email address: sampathkumarpb123@gmail.com